CHEMICAL ENGINEERING TRANSACTIONS
VOL. 113, 2024
A publication of AIDIC
The Italian Association of Chemical Engineering
Online at www.cetjournal.it
Guest Editors: Jeng Shiun Lim, Bohong Wang, Guo Ren Mong, Petar S. Varbanov

ISBN 979-12-81206-14-4; **ISSN** 2283-9216
DOI: 10.3303/CET24113060

Electrochemical Impedance Spectroscopy (EIS): an Efficient Method to Reveal Anion Storage Behaviour in Graphite Dual Ion Batteries

Sui Chang Ong, Zie Zin Khoo, Zhong Hong Lim, Woon Gie Chong*

School of Energy and Chemical Engineering, Xiamen University Malaysia, Bandar Sunsuria 43900, Malaysia.
woongie.chong@xmu.edu.my

Graphite dual-ion batteries (GDIBs) have gained attention in recent years due to their low cost and low environmental impact. The understanding of the anion storage behaviour which possesses a coupling mechanism of intercalation and capacitive processes remains unclear. Differentiating the nature of charge storage that are capacitive, pseudocapacitive, or battery-like behaviour of electrode materials is essential in structural design for optimized energy storage. Although conventional voltammetric analysis is a reliable approach to determine the capacitive contribution of charge-storing materials by measuring the current response against varying scan rates, it is usually time-consuming and requires a large number of complicated steps for analysis. In this study, a three dimensional (3D) Bode analysis is adopted as a complementary technique to characterize the capacitive contribution and oxidation kinetics of the fundamental anion storage processes. The anion storage mechanism of graphite electrodes in electrolytes containing anions with different ionic radius including PF_6^-, $TFSI^-$, $AlCl_4^-$ was investigated using AC impedance technique. Real capacitance C' versus frequency and the applied direct-current (DC) cell voltage are used as key descriptors to reveal the effect on the ionic sizes on the charge storage behaviour. 3D Bode plot of graphite electrode shows high C' at multiple voltages, indicating the staging mechanism which is consistent with the results obtained from cyclic voltammetric (CV) analyses. The proposed method in this work presents a facile characterization technique for anion storage processes compared to the complex in-situ microscopic and spectroscopic approaches.

1. Introduction

Battery technology development is progressing towards low-cost, facile fabrication of battery components, low and environmental impact (Jankuj et al., 2022). Tremendous efforts have been devoted to developing novel rechargeable batteries that operate using low-cost materials with high performance, and the graphite dual-ion battery (GDIB) is among them, demonstrating the desired properties. The concept of GDIB was first discovered in 1989 (Kravchyk et al, 2019), followed by the investigation of ionic electrolyte for GDIB, such as EMI^+, $DMPI^+$, $CF_3SO_6^-$, $AlCl_4^-$, $C_6H_5CO_2^-$, PF_6^- (Carlin et al., 1995), and BF_4^- (Sui et al., 2020). In later years, the concept of DIBs were extended to different monovalent and multivalent battery systems, including Na^+(Bordet et al., 2015), Al^{3+}(Lin et al., 2015), Ca^{2+}, K^+, Zn^{2+} based DIBs were reported (Chen et al., 2023). GDIB shows high potential in energy storage applications with its various electrolyte options; but its anion storage behaviours remains unclear (Rodríguez-Pérez et al, 2017). Among these DIBs, PF_6^- and $TFSI^-$ storage in graphite are widely studied thanks to their high intercalation voltage in graphite electrodes while $AlCl_4^-$ is well known for its ultrafast rechargeability in graphite-based electrodes (Ou et al., 2021).

Studies on anion intercalation are crucial for dual ion battery energy storage system. In-situ Raman spectroscopy were used in the investigation of $TFSI^-$ anion to study the structure and physical properties of the graphite electrode during $TFSI^-$ anion intercalation (Balabajew et al., 2016). X-ray Diffraction (XRD) were used to study the electrochemical intercalation, structural and compositional transformation of lithium bis(trifluoromethane)sulfonimide (LiTFSI) into graphitic carbons (Placke et al., 2014), X-ray photoelectron spectroscopy (XPS) was used to study the electrochemical lithium intercalation in the graphite anode (Momose

Paper Received: 25 March 2024; Revised: 5 August 2024; Accepted: 15 November 2024
Please cite this article as: Ong S.C., Khoo Z.Z., Lim Z.H., Chong W.G., 2024, Electrochemical Impedance Spectroscopy (EIS): An Efficient Method to Reveal Anion Storage Behaviour in Graphite Dual Ion Batteries, Chemical Engineering Transactions, 113, 355-360 DOI:10.3303/CET24113060

et al., 1997). Although all the mentioned methods are powerful for revealing anion intercalation, they are more costly, time-consuming, and resource-intensive compared to the EIS method proposed in this study.
The staging intercalation phenomenon characterizes the charge storage behaviour of graphite, which is presented by multiple intercalation peaks in CV curve. Anion intercalation behaviour in DIBs can be quantitatively and qualitatively analysed by using the equations $i = k_1 v + k_2 v^{0.5}$ and $i = a v^b$. The b value in the equation indicates the intercalation mechanisms such as pseudo-capacitive intercalation (PCI) and diffusion controlled intercalation (DCI). The b-value of various anions used in DIBs are summarized in table 1, where O_n represents the anion intercalation stage with increasing voltage. The b value varies as intercalation progresses, the contribution of the diffusion-controlled mechanism is significant, specifically at the highest voltage. The continuous anion intercalation/de-intercalation causes certain deterioration of the graphite structure, hindering the diffusion-controlled process which gives higher b values. Interestingly, larger anions $AlCl_4^-$ and $TFSI^-$ favours hybrid mechanism, while PF_6^- with smaller anion size of 3.5 Å facilitates its diffusion, leading to decreasing b value upon intercalation. The study of the ionic storage behaviour of electrode materials, such as PCI process or DCI process, is usually performed through CV with multiple scan rates to obtain the b value of respective anion batteries, making this approach time-consuming. To tackle this problem, this paper proposes a 3D Bode analysis as a fast screening technique to characterize capacitive contribution and reaction kinetics of the corresponding anion storage process in graphite cathode. Qualitative observation of the impedance trace via the Bode plots enabled the depiction of the sequence of charge motion-related phenomena contributing to the EIS response of the cell within specific frequency ranges. This preliminary qualitative analysis is useful for understanding the correlation between the anionic size and the storage mechanism, which is essential for optimizing the storage capacity of DIBs.

Table 1: b-values and anionic size of various anion intercalation in graphite.

Anion	b value	Anion intercalation mechanism	Anionic Size (Å)	Ref
PF_6^-	O1=0.75 O2=0.94 O3=0.85 O4=0.66	Hybrid mechanism Intercalation at dominant stage O1 and O4	3.5	(Wei et al., 2023)
$TFSI^-$	O1=0.87 O2=0.82	Hybrid mechanism	8.0	(Zheng et al., 2021)
$AlCl_4^-$	O1=0.77 O2=0.60	Hybrid mechanism	5.3	(Chong et al., 2022)

2. Material and methods

2.1 Preparation of electrolytes

The preparation of electrolytes was carried out in glovebox filled with argon gas. High concentration electrolytes were prepared for the Li-based electrolyte to prevent the decomposition of ethyl methyl carbonate (EMC) and corrosion on the aluminium current collector due to the high working voltage of up to 5 V. The electrolyte of 3.5 M LiTFSI, Lithium hexafluorophosphate ($LiPF_6$, Sigma Aldrich) were prepared by dissolving the salts in EMC separately. The electrolyte containing $AlCl_4^-$ was prepared by mixing triethylammonium chloride (Et_3NHCl, 99 +%, Acros Chemicals) with anhydrous aluminum chloride ($AlCl_3$, 99.999 %, Acros Chemicals) with molar ratio of 1:1.3, to form a balanced concentration of $AlCl_4^-$ and $Al_2Cl_7^-$, which are the active anions in the redox reactions.

2.2 Electrode preparation

Commercial graphite, KFG-6 from Timcal was used as cathode active material. A commercial formulation was used to prepare the electrodes, consisting of KFG-6, Super P as the carbon additive, and polyvinylidene fluoride (PVDF) as the binder, with a mass ratio of 8:1:1. N-Methyl-2-pyrrolidone (NMP) was added to dissolve PVDF in the mixture to form a homogeneous slurry. The slurry was coated onto an aluminium foil using the doctor-blade casting method, with an initial wet thickness of 20 µm. The dried electrode was punched into circular discs with a diameter of 12 mm.
The 2032 coin cells were prepared in a half cell setup with lithium foil as anode, two layers of glass fiber separator (Whatman 934-AH) soaked with $LiPF_6$ or LiTFSI electrolyte and the graphite cathode. For $AlCl_4^-$ containing electrolyte, the anode was replaced by aluminium foil, and the electrolyte used was $AlCl_3/Et_3NHCl$.

3. Experimental

For this study, the anion storage ability of graphite electrode with $LiPF_6$, LiTFSI, and $AlCl_3$ electrolyte were accessed via cyclic voltammetry(CV) over VersaSTAT 4 electrochemical workstation in a half-cell configuration at a scan rate of 0.1 mV s^{-1}. The voltage range was varied between 3.0-5.0 V for the lithium-based electrolyte system and 0.5-2.5 V for aluminium-based electrolyte. The CV configuration obtained from $LiPF_6$, shown in Figure 1a, indicates a battery-like mechanism, where several prominent anodic and cathodic peaks are corresponding to the oxidation and reduction of PF_6^- at graphite electrodes. The voltage of each oxidation peak of $LiPF_6$ are listed as 4.51, 4.63, 4.79, and 4.98 V.

3.1 Real component of Capacitance

While the Bode plot analysis, an RMS voltage (V_{RMS}) with an amplitude of 10 mV was applied to the coin cells within frequency (f) range from 5 mHz to 0.1 MHz. The voltage ranges for $LiPF_6$ and LiTFSI were 3.0 to 5.0 V, while voltage range for $AlCl_3$ were 0.7 to 2.4 V. The real component of capacitance is C', and it is calculated from the impedance data from 10 mHz to 10 Hz. The real components of impedance are Z', while having a relationship with C', which is the real capacitance as shown in Eq(1).

$$C' = \frac{-Z'(\omega)}{\omega|Z(\omega)|^2} \tag{1}$$

where ω is the angular frequency obtained from Bode plot analysis. The capacitive region in the Nyquist plot provides information solely about the fast processes occurring within the cell which is a reliable method to understand the capacitive performance of a material tested in the coin cell (Taberna et al., 2003).
This paper studies the impedance data in traditional 2 dimensional Bode plot, which is real capacitance versus frequency, obtained at a desired cell voltage range which determined by the working voltage of specific chemical reaction. The mid-point between oxidation and reduction peaks from the cyclic voltammograms was taken as the half-wave potential, $E_{0.5}$. The equation is shown in Eq(2).

$$E_{0.5} = \frac{E_a + E_c}{2} \tag{2}$$

where E_a is the anodic peaks, and E_c is the cathodic peaks. The formula above is usually performed to conclude the reversibility of the electrochemical battery system according to the half-wave potential at the increasing scan rates.(Espinoza et al., 2019) Hence, the $E_{0.5}$ was used as a starting point to study the electrochemical characteristics of $LiPF_6$, LiTFSI, and $AlCl_3$, where the corresponding $E_{0.5}$ value were 4.6, 4.5, and 2.0 V.

3.2 CV curves

Figure 1a-c shows the typical battery-like CV curves of graphite tested against $LiPF_6$, LiTFSI, and $AlCl_3$ electrolytes, with all have their corresponding oxidation and reduction peaks at the specific voltage windows. The cathodic scan of the cell in $LiPF_6$ electrolyte revealed three main oxidation peaks between 3.0 and 5.0 V as shown in Figure 1(a), correlate with stage 4 and stage 3 intercalation process, subsequently, stage 2 intercalation occurs at 4.98 V. CV curve obtained from graphite electrode in LiTFSI electrolyte shows two oxidation peaks at 4.67 V corresponds from the stage 4 $TFSI^-$ anion intercalation, and the oxidation peak exist at 5.01 V were associated to the stage 3 $TFSI^-$ intercalation, which resembles the staging mechanism of anion storage in graphite (Heckmann et al., 2018). It should be mentioned that the redox reaction is usually depicted by the sharp peaks in CV. The broad peak observed between 3.5-3.6 V, characterized by a significantly lower current density, suggests a capacitive storage mechanism. This mechanism appears to initiate with capacitive behaviour, followed by intercalation at 3.98 V.
Figure 1(c) shows the oxidation peaks was ascribed to the surface adsorption of the $AlCl_4^-$ anion on the KFG-6 graphene crystals during charging process; while the highest oxidation peak exists at 2.39 V, suggesting the diffusion-controlled stage 4 $AlCl_4^-$ intercalation into graphene interlayer.

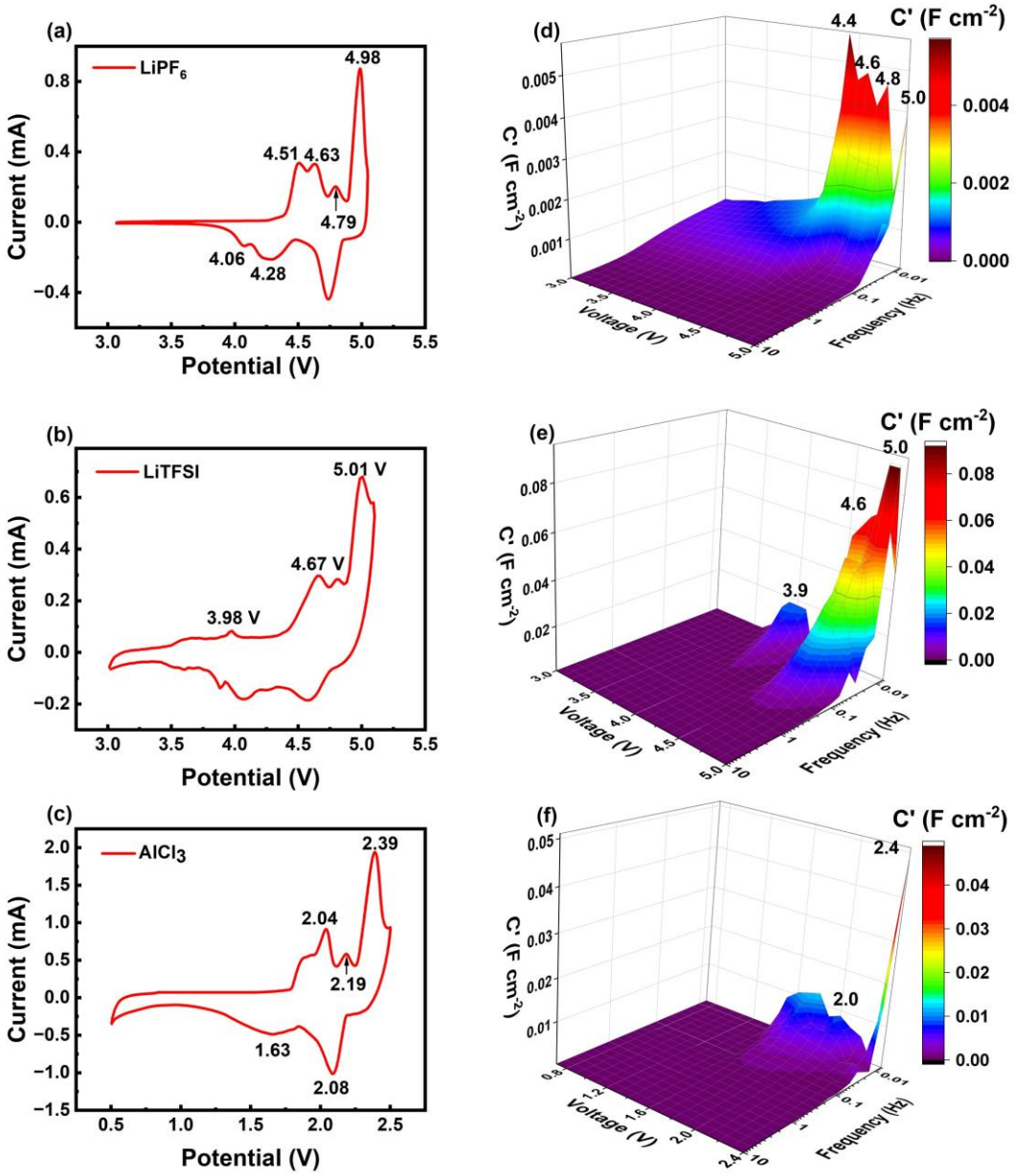

Figure 1: (a-c) Cyclic voltammograms and (d-f) Bode plots of the real area-normalized capacitance of graphite electrodes based on the a) $LiPF_6$, b) LiTFSI, c) $AlCl_3$ electrolytes.

3.3 Bode Plots

With increasing frequency in the Bode plot analysis from 5 mHz to 0.1 MHz, the time scale of the electrochemical process of real capacitance retention were obtained, and it was found that there are multiple peaks obtained in the Bode plot of the electrolytes. Figure 1d-f show the peaks of frequency response to the real area-normalized capacitance for $LiPF_6$ are 4.4, 4.6, 4.8 and 5.0 V; while the peaks of the C' for LiTFSI are 3.9, 4.6, and 5.0 V; the peaks of the C' for $AlCl_3$ are 2.0 and 2.4 V which are consistent with reaction voltages as shown in the CV curves.

This is crucial as usual CV scanning at an accurate rate of 0.1 mV/s requires long hours to perform analysis, and this is usually accompanied with multiple scan rates, which requires several days. The Bode plot analysis proposed in this study revealed the charge storage characteristics of the battery, requiring only 20 h (less than a day) for the entire analysis. This method can forecast the behaviour of the samples by identifying the position of the oxidation peaks.

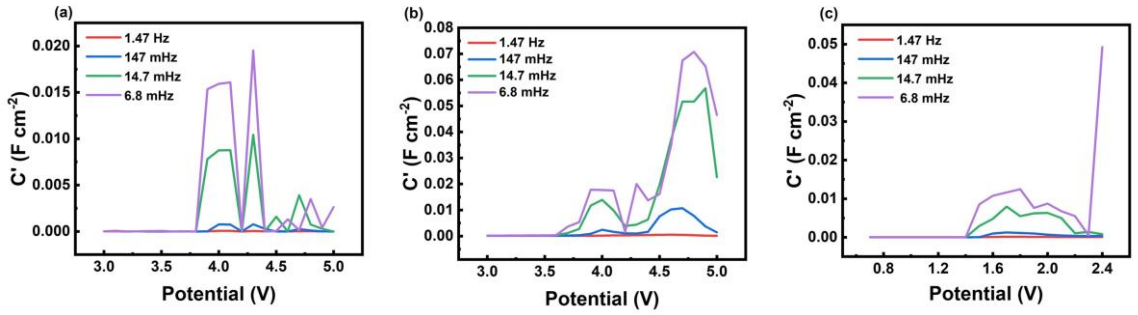

Figure 2: The real area-normalized capacitance of graphite electrodes based on a) $LiPF_6$, b) LiTFSI, c) $AlCl_3$ electrolytes.

By analysing EIS data which was translated into the 3D Bode plots, the charge-storage dynamics of the anions were extensively studied, it should be mentioned that C′ is the dependent variable, while the manipulated variables are the frequency and cell voltage, which are different for different electrolyte systems. Figure 1d-f presented battery-like mechanism, where observable high C′ is detected at the voltage where oxidation occurs, Meanwhile, the C' is negligible at other voltage range. For capacitive materials, the C' will be almost constant across the entire voltage range in the Bode plots. A magnified view of the C' response to voltage at selected frequency of 6.8, 14.7, 147 and 1470 mHz were presented in Figure 2. The C' response was observable only in the low-frequency range, confirming that the process is governed by the diffusion of the redox species from the bulk solution to the electrode surface (Alexandros et al., 2023).

Figure 1d and 2a show a marginally increase in capacitance retention with $C' < 0.0015\ \mathrm{F\ cm^{-2}}$ for PF_6^- when voltage was sweep from 3.0-5.0 V, suggesting the hybrid storage mechanism for the region outside the oxidation voltage. The sharp peaks are corresponding to the faradaic reactions during the PF_6^- intercalations. Figure 1e-f and 2b-c show island-like weak peaks in the first oxidation peak for both $TFSI^-$ and $AlCl_4^-$ system, indicating the initial intercalation is dominated by PCI process (higher b values, see Table 1). This is followed by DCI (lower b values), which is presented as a well-defined peak in the subsequent intercalation stage. It should be mentioned that this behaviour was only seen for $TFSI^-$ and $AlCl_4^-$ which have larger anionic size than the counterpart. In addition, the broad peak found between 3.5-3.6 V in the Figure 1b was not seen in Figure 1e, which was resulting from the low capacitance retention of the capacitive process, the C' value is too marginal to be observable and tends to be overlapped by the high C' of the dominant battery-like process at 3.98 V. These findings validate that anions exhibit complex charge-storage dynamics which involve both capacitive-driven and rate-determining redox reactions. The correlations between the ionic size and the capacitive contribution were qualitatively elucidated.

4. Conclusions

In this work, 3D Bode analysis were adopted to analyse charge storage mechanism of the multi-stage intercalation of anions, which offers a complementary technique to forecast the behaviour of graphite electrode. The Bode plot analysis of the graphite electrodes based on $LiPF_6$, LiTFSI, and $AlCl_3$ electrolytes with multiples peaks confirmed the battery-like response of anions storage in graphite. In particular, the battery response of the three different anions were illustrated by the well-defined peaks at their characteristics oxidation voltage. The overlapped region between PCI and DCI process were revealed by the real area-normalized capacitance C', which emerged as a broad peak in the 3D Bode plots. The capacitance retention of the PCI dominated-oxidation reaction of large anions ($TFSI^-$ and $AlCl_4^-$) show distinct contrast to the DCI-dominated process of PF_6^- .This electroanalytical approach offers a promising direction for characterizing rapid anion storage processes. The knowledge obtained from potentiostatic impedance measurements serve as a reference for analyzing EIS data sets. This finding reduces the time required to study the anion storage process in DIBs, and this lowers the cost of studying and characterizing DIBs.

Acknowledgements

This work was supported by Fundamental Research Grant Scheme by Ministry of Higher Education Malaysia (Grant No: FRGS/1/2020/STG05/XMU/02/3) and Xiamen University Malaysia Research Fund (Grant No. XMUMRF/2019-C4/IENG/0021).

References

Alexandros C.L., Mamas T.P., 2023, Electrochemical impedance spectroscopy- a tutorial, ACS Measurement Science, 3, 162-193.

Balabajew M., Reinhardt H., Bock N., Duchardt M., Kachel S., Hampp N., Roling B., 2016, In-situ raman study of the intercalation of bis(trifluoromethylsulfonyl)imid ions into graphite inside a dual-ion cell, Electrochimica Acta, 211, 679-688.

Bordet F., Ahlbrecht K., Tübke J., Ufheil J., Hoes T., Oetken M., Holzapfel M., 2015, Anion intercalation into graphite from a sodium-containing electrolyte, Electrochimica Acta, 174, 1317-1323.

Carlin R., De-Long H., Fuller J., Lauderdale W., Naughton T., Trulove P., Bahn C., 1995, Dual intercalating molten electrolyte batteries. MRS Online Proceedings Library (OPL), 393, 201.

Chen C., Lee C.S., Tang Y.B., 2023, Fundamental understanding and optimization strategies for dual-ion batteries: a review, Nano-Micro Letters, 15(1), 121.

Chong W.G., Ng Z.I., Yap S.L., Foo C.Y., Jiang H., Guo H., Lim H.N., Huang N.M., 2022, Facile fabrication of freestanding graphene nanoplatelets composite electrodes for multi battery storage, Materials Today Communications, 31, 103782.

Espinoza E.M., Clark J.A., Soliman J., Derr J.B., Morales M., Vullev V.I., 2019, Practical aspects of cyclic voltammetry: how to estimate reduction potentials when irreversibility prevails, Journal of the Electrochemical Society, 166(5), H3175-H3187.

Heckmann A., Meister P., Kuo L.Y., Winter M., Kaghazchi P., Placke T., 2018, A route towards understanding the kinetic processes of bis(trifluoromethanesulfonyl)imide anion intercalation into graphite for dual-ion batteries, Electrochimica Acta, 284, 669-680.

Jankuj V., Spitzer S.H., Krietsch A., Štroch P., Bernatík A., 2022. Safety of alternative energy sources: A review,Chemical Engineering Transactions, 90, 115-120.

Kravchyk K.V., Kovalenko M.V., 2019, Rechargeable dual-ion batteries with graphite as a cathode: key challenges and opportunities, Advanced Energy Materials, 9(35), 1901749.

Lin M.C., Gong M., Lu B., Wu Y., Wang D.Y., Guan M., Angell M., Chen C., Yang J., Hwang B.J., 2015, An ultrafast rechargeable aluminium-ion battery, Nature, 520(7547), 324-328.

Momose H., Honbo H., Takeuchi S., Nishimura K., Horiba T., Muranaka Y., Kozono Y., Miyadera H., 1997, X-ray photoelectron spectroscopy analyses of lithium intercalation and alloying reactions on graphite electrodes, Journal of Power Sources, 68(2), 208-211.

Ou X., Gong D., Han C., Liu Z., Tang Y., 2021, Advances and prospects of dual-Ion batteries, Advanced Energy Materials, 11(46), 2102498.

Placke T., Schmuelling G., Kloepsch R., Meister P., Fromm O., Hilbig P., Meyer H., Winter M., 2014, In situ X-ray diffraction studies of cation and anion intercalation into graphitic carbons for electrochemical energy storage applications, Zeitschrift für anorganische und allgemeine Chemie ZAAC, 640(10), 1996-2006.

Rodríguez-Pérez I.A., Ji X., 2017, Anion hosting cathodes in dual-ion batteries, ACS Energy Letters, 2(8), 1762-1770.

Sui Y., Liu C., Masse R.C., Neale Z.G., Atif M., AlSalhi M., Cao G., 2020, Dual-ion batteries: the emerging alternative rechargeable batteries, Energy Storage Materials, 25, 1-32.

Taberna P., Simon P., Fauvarque J.F., 2003, Electrochemical characteristics and impedance spectroscopy studies of carbon-carbon supercapacitors, Journal of the Electrochemical Society, 150(3), A292.

Wei Y., Tang B., Liang X., Zhang F., Tang Y., 2023, An ultrahigh-mass-loading integrated free-standing functional all-carbon positive electrode prepared using an architecture tailoring strategy for high-energy-density dual-ion batteries, Advanced Materials, 35(30), 2302086.

Zheng Y., Qian T., Ji H., Xia X., Liu J., Zhu Y., Yan C., 2021, Accelerating ion dynamics under cryogenic conditions by the amorphization of crystalline cathodes, Advanced Materials, 33(35), 2102634.